A Journal of the Gesellschaft Deutscher Chemiker

Angewandte International Edition Chemie

GDCh

www.angewandte.org

Accepted Article

Title: Aqueous Batteries Operated at - 50 °C

Authors: Qingshun Nian, Jiayue Wang, Shuang Liu, Tianjiang Sun, Shibing Zheng, Yan Zhang, Zhanliang Tao, and Jun Chen

To be cited as: *Angew. Chem. Int. Ed.* 10.1002/anie.201908913
Angew. Chem. 10.1002/ange.201908913

Link to VoR: http://dx.doi.org/10.1002/anie.201908913
http://dx.doi.org/10.1002/ange.201908913

WILEY-VCH

10.1002/anie.201908913

WILEY-VCH

RESEARCH ARTICLE

Aqueous Batteries Operated at - 50 ℃

Qingshun Nian†, Jiayue Wang†, Shuang Liu, Tianjiang Sun, Shibing Zheng, Yan Zhang, Zhanliang Tao, and Jun Chen*

Dedicated to the 100th anniversary of Nankai University

Abstract: *Insufficient ionic conductivity and freeze of electrolyte at low temperature (low-T) are considered the main problems for low-T electrochemical energy storage. Here, the electrolyte with freezing point lower than -130 ℃ is developed by using dimethyl sulfoxide (DMSO) as an additive with the molar fraction of 0.3. The 2M-0.3 electrolyte (by adding DMSO with a molar fraction of 0.3 to the aqueous solution of 2 M $NaClO_4$) exhibits sufficient ionic conductivity of 0.11 mS cm^{-1} at -50 ℃. The combination of spectral investigations and molecular dynamics (MD) simulation reveals that the hydrogen bonds are stably formed between DMSO and water molecules and this is taking the role for the electrolyte working at an ultra-low-T. Using DMSO as the electrolyte additive, the aqueous rechargeable alkali-ion batteries (AABs) can work well even at -50 ℃. This work provides a simple and effective strategy to develop low-T AABs.*

Introduction

Owing to the high ionic conductivity, environmental friendliness, and low cost of the electrolyte, aqueous alkali-ion (Li^+, Na^+, and K^+) batteries (AABs) have aroused an increasing attention in recent years.[1] At present, it was reported that the minimum temperature for AAB work is -20 ℃.[2] It is difficult for AABs to meet the demands in fields such as electric vehicles, aerospace technology and military. A common issue is that the AABs sacrifice most of their capacity and power when the temperature drops. The insufficient ionic conductivity and freezing of electrolyte are generally considered as the main reasons for this issue.[3] Therefore, improving the low temperature (low-T) performance is essential for the practical application of AABs. Serving as the ionic conductor, electrolyte has great impact on the integral performance of the battery. Thus, optimizing electrolyte to improve the battery low-T performance has been proved to be a feasible technical approach. Over the past years, various approaches regarding electrolyte renovation to overcome the low-T issue have been reported (e.g., using low freezing point electrolyte solvent [4] and developing electrolyte additives,[5] etc.) Electrolyte additives play an increasingly important role in improving the battery performance.[6] Due to the characteristics of "small dosage" and "quick effect", additives can significantly improve the low-T performance of battery without increasing the production cost and changing the production process. Currently, research on low-T additives mainly focuses on non-aqueous batteries,[7] and less attention has been paid to aqueous batteries. Therefore, it is necessary to develop additives to improve the low-T behavior of aqueous electrolyte.

Dimethyl sulfoxide (DMSO) is a sulfur-containing compound with a molecular formula of $(CH_3)_2SO$. It possesses high polarity, high boiling point, and good thermal stability. DMSO can dissolve most types of inorganic salts, and thus be commonly used as an electrolyte solvent.[8] It's worth noticing that DMSO can mix with water in any ratio. Water is the donor and acceptor of hydrogen bond (HB) simultaneously, while DMSO can only be HB acceptor. This difference gives rise to a variety of important properties of water/DMSO binary solutions.[9] One of the fascinating applications of water/DMSO binary solution is the low melting point to preserve biological systems. In 1959, Lovelock reported that the DMSO can serve as a preservative and freezing medium for biological tissues.[10] Afterward, Havemeyer (1966) studied a series of different molar fraction water/DMSO mixtures (χ), and found that the apparent freezing temperature of water/DMSO mixture (χ_{DMSO}=0.30) could be as low as ~ -140 ℃, which is lower than the melting points of both components (18.9 ℃ for DMSO and 0 ℃ for water).[11] Subsequently, Rasmussen (1968) illustrated the phase diagram of a series of DMSO-water eutectic mixtures with different molar fractions.[12] Considering the extremely low freezing point, the water/DMSO hybrid system can be used to develop low-T electrolyte for aqueous batteries.

Herein, we construct the aqueous electrolyte with low freezing point by adding DMSO to aqueous solution of 2 M $NaClO_4$. The DMSO molar fraction is 0.3 (χ_{DMSO}=0.3), and the freezing point of the electrolyte is lower than -130 ℃. Ionic conductivity of the electrolyte is 0.11 mS cm^{-1} even at ultra-low temperature of -50 ℃. Measurement of spectral investigation and molecular dynamics (MD) reveal the underlying mechanism for the low freezing point of the electrolyte. We found that the stable HBs form between DMSO and water molecules, where DMSO acts as the HB acceptor while water serves as the donor. More importantly, AABs assembled by the DMSO-added electrolyte can work well even at -50 ℃. Furthermore, the capacity at -50 ℃ maintains ~60 % of that at 25 ℃. This design makes it possible for AABs to operate properly at low-T conditions. The superior low-T performance of the electrolyte will eventually promote the application of AABs in fields such as electric vehicles, aerospace technology and military.

Results and Discussion

It is known that the freezing points of pure DMSO and water are 18.9 ℃ and 0 ℃, respectively. DMSO and water can be mixed to achieve low freezing point. In order to ensure the feasibility of such mixed electrolyte solvent at low-T, the freezing point is explored by differential scanning calorimetry (DSC). Figure 1a displays DSC results of the electrolyte solvent (salt-free) with χ_{DMSO}=0.3 (by adding DMSO with a mole fraction of 0.3 to the aqueous solution). The lowest freezing point is -130 ℃, which is beneficial for batteries to operate at ultra-low T. For the system with DMSO molar ratio of 0.3, we tried to determine the solvates (salt-contained) freezing point by DSC. However, the DSC data shows no exothermic peak, indicating that the solvates (salt-contained) have freezing point below -150 ℃. DSC cooled with

Q. Nian, S. Liu, T. Sun, S. Zheng, Prof. Z. Tao*, and Prof. J. Chen
Key Laboratory of Advanced Energy Chemistry (Ministry of Education), College of Chemistry, Nankai University
Tianjin 300071 (China)
E-mail:taozhl@nankai.edu.cn
Dr. J. Wang
State Key Laboratory of Molecular Reaction Dynamics, Dalian Institute of Chemical Physics (DICP)
Chinese Academy of Sciences
Dalian 116023 (China)
Prof. Y. Zhang
Institute of Molecular Sciences and Engineering
Shandong University
Qingdao 266237 (China)
† These authors contributed equally to this work.

Supporting information for this article is given via a link at the end of the document.

10.1002/anie.201908913

liquid nitrogen can not work at temperatures lower than -150 ℃. Thus, the freezing point of the solvates cannot be determined. In order to visualize the freezing point of the electrolyte, we decided to start from the freezing point of the pure solvents(salt-free), and then used the "colligative properties of the solution" to determine the freezing point of the solvates (salt-contained), which is lower than that of pure solvents (-130 ℃). At the same time, the freezing points of pure DMSO, pure water, χ_{DMSO}=0.1 and χ_{DMSO}=0.5 are also determined (Figure S1), whose freezing points are 18.9 ℃, 0 ℃, -31 ℃ and -69.3 ℃, respectively. Thus, the χ_{DMSO}=0.3 electrolyte solvent (salt-free) can achieve the lowest freezing point, which is more suitable for low-T applications. In order to observe the freezing point of pure DMSO solution, pure water and χ_{DMSO}=0.3 electrolyte solvent (salt-free) more intuitively, morphology changes of these electrolyte solvents with the temperature change are observed using a polarizing microscope according to the isotropy and anisotropy of the liquid before and after freezing. As shown in Figure 1b, the pure DMSO starts to freeze at 18 ℃, and pure water starts to freeze at ~0 ℃. After mixing, the χ_{DMSO}=0.3 electrolyte solvent (salt-free) does not freeze until at ultra-low temperature of -130 ℃. This result is consistent with the DSC data.

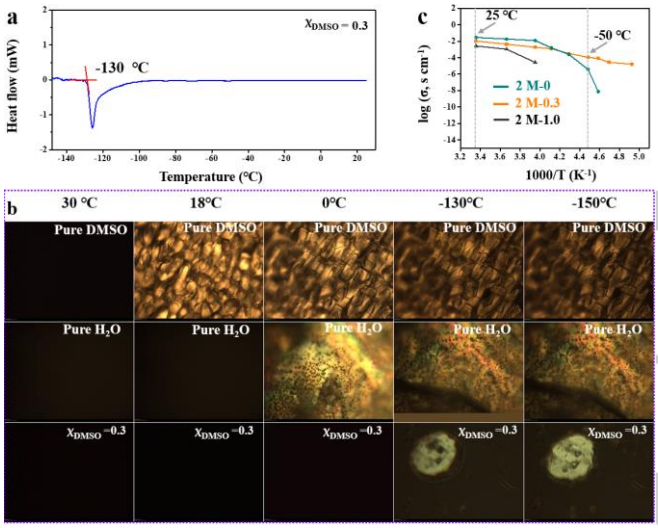

Figure 1. Characteristics of the electrolytes, (**a**) DSC for χ_{DMSO}=0.3 electrolyte solvent; (**b**) Optical photos at different temperatures from polarized light microscopes; (**c**) Temperature-dependent ionic conductivity investigation.

The temperature-dependent ionic conductivity was also studied (Figure 1c). The ionic conductivity of 2M-0 (2 M $NaClO_4$ no DMSO) electrolyte is 2.9 mS cm^{-1} at 25 ℃. However, the ionic conductivity can't be obtained when temperature is below -40 ℃. On the contrary, the 2M-0.3 (by adding DMSO with a molar fraction of 0.3 to the aqueous solution, 2 M $NaClO_4$) electrolyte exhibits the highest ionic conductivity of 0.11 mS cm^{-1} at -50 ℃ because the addition of DMSO reduces the freezing point of the electrolyte.

The spectral investigation results summarized in Figure 2 show the stretching vibration alteration for S=O, CH_3 and O-H of the electrolyte solvents with different DMSO molar fraction. Figure 2a-c present the local Raman spectrum of the electrolyte solvents with different DMSO molar fraction, and the full Raman spectrum is displayed in Figure S2. From Figure 2a, it can be found that the electrolyte solvents with different molar fraction of DMSO display unique stretching mode of sulfoxide (S=O) group within 1000-1100 cm^{-1}. As the concentration of DMSO increases, the spectral bands are shifted to the higher wavenumber region (blue shift). Such blue shift trend could be explained by the interaction between the O-H bond in the water molecule and the S=O double bond in DMSO, i.e. S=O···H-O.[13,14] Moreover, the Raman band of S=O double bond in water/DMSO solution is firstly widened and then narrowed with the increase of DMSO concentration. The wide spectrum band is composed of two parts, including the low frequency part that interacts with O-H bond of water, and the high frequency part that does not interact with O-H bond of water.[15,16] The stretching vibration of methyl (CH_3) is shown in Figure 2b. The symmetric and asymmetric stretching vibrations of CH_3 are distributed at 3008 cm^{-1} and 2921 cm^{-1}, respectively. As the concentration of DMSO increases, strong HBs between S=O and O-H are formed and the charges are redistributed. As a result, the Raman peak of the CH_3 has shifted to a lower wavenumber. On the contrary, the O-H stretching vibration peak moves to a higher wavenumber as the DMSO concentration increases (Figure 2c). This result indicates that the hydrogen-bonding interactions among water molecules which are strongly incorporated in the water HB network have been weakened in the DMSO-Water mixtures.[16] Figure 2d-e show the local FT-IR spectrum of DMSO-Water mixtures with different DMSO molar fraction, and full FT-IR spectrum is displayed in Figure S3. Changes of the corresponding peaks in FT-IR spectra are in consistent with that from the Raman spectra. As the DMSO molar fraction increases, the S=O stretches move to higher wavenumbers, implying that the hydrogen-bonding network in which DMSO and water molecules are participated in becomes stronger (Figure 2d).[17] The enlarged CH_3 peaks (FT-IR) are illustrated in Figure 2e. The symmetric and antisymmetric CH_3 stretching modes in the region of 2910 cm^{-1}-3000 cm^{-1} have shifted to the red side when DMSO is added. These results can be recognized from the Raman spectra. Figure 2f displays the experimental spectra in the OH stretching region. With the increase of DMSO concentration, the overall bands show apparent blue-shift, which is in agreement with the result in the Raman spectra (Figure 2c). The possible explanation for the above results is the HB formation between DMSO and water molecules. In order to verify that the HB formation would induce vibration shift, NMR detection is also applied. Figure S4 shows the ^1H NMR chemical shifts of all electrolyte solvent samples. A significant shift has been observed for the water peak with the addition of DMSO, further demonstrating the HB formation between DMSO and water. Theoretically, the inter-molecular HBs formation between DMSO and water would damage the HB network within water molecules and prevent the HB grids from construction in ice crystals.[13,18] Thus, the electrolyte with DMSO addition may possess a decreased freezing point.

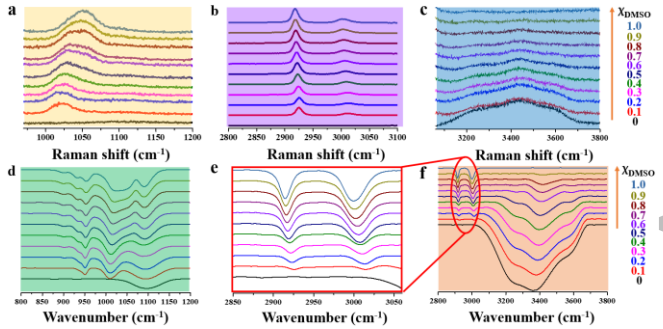

Figure 2. Raman spectroscopy of different DMSO molar fractions of water/DMSO solutions (**a**) S=O band; (**b**) CH_3 stretching modes of DMSO; (**c**) OH stretching bands of water. FT-IR of water and DMSO at different mole fractions (**d**) S=O band; (**e**) CH_3 stretching modes of DMSO; (**f**) OH stretching band of water.

Furthermore, Molecular Dynamics (MD) simulation is performed to understand the electrolyte solvent with different molar fractions of DMSO. After the 10 ns MD simulation, we

10.1002/anie.201908913

analyzed the HB formation of the different DMSO-Water mixtures. Simulation details are summarized in Table S1. Figure 3a shows the averaged number of HBs between DMSO and water molecules divided by DMSO quantity for each system. It is clear that, except χ_{DMSO}=0.1 and 0.2, the averaged HB number of other systems would become stable after 4.5 ns. Since the systems with DMSO fraction of 0.1 and 0.2 haven't reached equilibrium of HB formation states after sufficient simulation time (10 ns), indicating that they may not possess the stable HB bond formation states. We would exclude these two systems in the latter discussion. Energetically, HB between DMSO and water is more stable than that within water molecules. The strongest interactions have been found between the DMSO oxygen atom and the water-hydrogen atom.[19] Early neutron scattering experiments and simulation studies have identified the co-existence of 1DMSO-2Water and 2DMSO-1Water molecular aggregates formed by strong HB, of which the first aggregate formation have impact on thermodynamics, dielectric constant, viscosity and dielectric relaxation times,[20] while the latter may be manifested in physicochemical qualities sensitive to short-time dynamics.[21] As 1DMSO-2Water aggregate plays the dominant role, we summarized the amount of DMSO molecules in 1DMSO-2Water HB formation and 2DMSO-1Water. The ratio value, which takes the amount of DMSO molecules in the 1DMSO-2Water formation as divisor and the 2DMSO-1Water formation as dividend, are plotted against the gradient changed DMSO fraction. The result is presented in Figure 3b. It can be illustrated that, system with χ_{DMSO} =0.3 have the most of their DMSO-Water HB in the form of 1DMSO-2Water. With the large portion of 1DMSO-2Water HB formation, more water molecules would be trapped in the DMSO-Water aggregates instead of Water-Water aggregates. This prevents water molecules from forming the ordered hydrogen-bond-network which is the geometrical basis for crystallization.

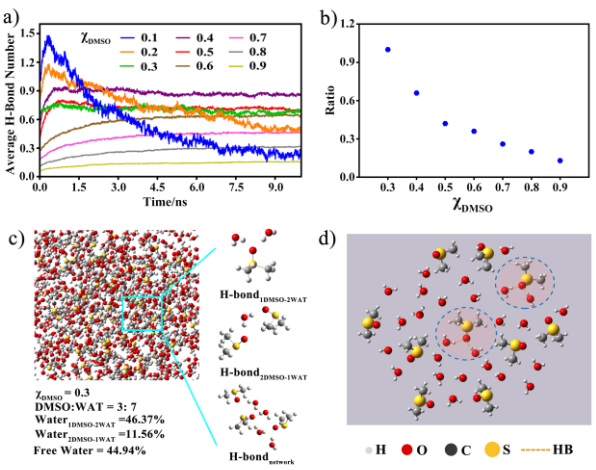

Figure 3. (**a**) Averaged HBs number for each system for 10ns simulation time; (**b**) Ratio value, which takes the amount of DMSO molecules in the 1DMSO-2Water formation as divisor and the 2DMSO-1Water formation as dividend, are plotted against the gradient changed system fraction; (**c**) Conformation analysis of the system with χ_{DMSO} =0.3 from MD simulations; (**d**) Local structure of the system with χ_{DMSO} =0.3 from MD simulations.

System with χ_{DMSO} =0.3 has been identified to reach rather stable state for DMSO-Water HB formation and have most of its DMSO molecules in 1DMSO-2Water aggregates according to the simulation studies. We also performed conformation analysis for this particular system, and results are displayed in Figure 3c. Local structure of system with χ_{DMSO} =0.3 given by MD is shown in Figure 3d. The final frame from 10ns MD simulation for the system with χ_{DMSO} =0.3 is extracted, of which one specific field vision is shown as the upper left diagram in Figure 3c. In this vision scope, water molecules which have participated in the 1DMSO-2Water bond formation occupy ~46% of all water, while those contributing to 2DMSO-1Water have consumed only ~12%. Besides the two identified HB formation between DMSO and water molecules, as shown in the upper and middle right in Figure 3c, there exists a network-like fashion that inter-connect the two HB form (shown in bottom right in Figure 3c). The previous quantum chemical studies have illustrated that the 1DMSO-2Water HB formation involved in the network/cluster do not have mininum energy configurations.[19] Many configurations lie in the same interaction energy range. In this way, the mixture would not generate crystal-like ordered structure at low temperature and thus helps to decrease the freezing point.

In general, the mechanism interprets the reason to produce the lowest freezing point. The system with χ_{DMSO} =0.3 may lies in the inhibition of crystal-like ordered structure. It reaches a rather stable state in which DMSO and water molecules could form strong HB and has a rather large proportion of DMSO occupies in the 1DMSO-2Water HB formation. The stable state and large portion of 1DMSO-2Water HB prevent relatively large portion of water molecules from forming ordered network for crystallization and help to form more 1DMSO-2Water HB involved network/cluster with diverse configurations. This prohibits the generation of crystal-like ordered structure.

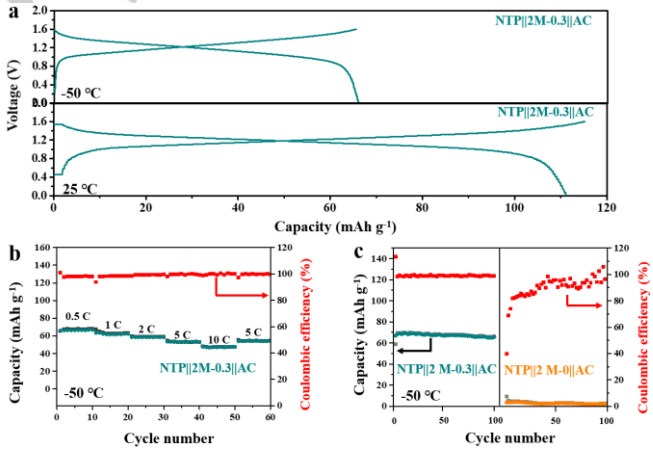

Figure 4. Electrochemical performance of the rechargeable NTP||2M-0.3||AC battery; (**a**) Charge-discharge curve tested at 25 ℃ and -50 ℃; (**b**) Rate performance at the ultra-low temperature of -50 ℃; (**c**) The cycle performance of NTP||2M-0.3||AC battery and NTP||2M-0||AC battery tested at -50 ℃.

Using the above 2M-0 and 2M-0.3 as electrolyte we fabricated the full cell based on $NaTi_2(PO_4)_3$@C (NTP) as anode material and activated carbon (AC) as cathode material. The morphologies of NTP are investigated via scanning electron microscope (SEM) and transmission electron microscopy (TEM). Figure S5 clearly shows the hierarchical micro-flower morphology of NTP and the micro-flowers have an average diameter *ca.* 5 μm. Figure S6a demonstrates the cyclic voltammetry (CV) measurement of NTP with 2M-0.3 electrolyte at a scan rate 0.5 mV s^{-1}. This NTP exhibits a pair of redox peaks in good symmetry at -0.7 V and -0.8 V vs. Ag/AgCl (1 M KCl, 0.2224 V vs. NHE) demonstrates the compatibility with the 2M-0.3 electrolyte. Figure S6b displays the NTP charge/discharge voltage platform at a rate of 0.5 C. The results indicate that the NTP has good correspondence with the position of the redox peak in the CV curves. The NTP||2M-0.3||AC battery exhibits 68 mAh g^{-1} at a rate of 0.5 C (1 C=133 mA g^{-1}) at -50 ℃ (Figure 4a), corresponding to a 61 % capacity retention of that at 25 ℃. It can be easily detected from Figure 4b and 4c that

NTP||2M-0.3||AC battery displays excellent rate and cycle performance at -50 ℃. However, it is worth noting that NTP||2M-0||AC battery cannot properly work at -50 ℃. Figure S7 shows the charge/discharge curves of NTP||2 M-0||AC full cell at 25 ℃ and -50 ℃. The experimental results obtained from the NTP||2M-0||AC full cell indicate that it does not work properly at -50 ℃. Figure S8 displays NTP||2M-0.3||AC and NTP||2M-0||AC battery which show excellent cycle performance at 25 ℃. At the same time, NTP||2M-0.3||AC and NTP||2M-0||AC battery still show excellent cycle and rate performance at high temperature of 45 ℃ (Figure S9). It is revealed that the improvement in low-T will not adversely influence the batteries at high temperature and rate capability. Furthermore, the DMSO included in low-T additive is also applied to aqueous lithium ion batteries (ALIBs) and aqueous potassium ion batteries (APIBs). We fabricated ALIBs with 0.5 M Li_2SO_4 and 0.5 M Li_2SO_4-0.3 (adding DMSO with a mole fraction of 0.3 to the aqueous solution of 0.5 M Li_2SO_4) as the electrolyte, $LiTi_2(PO_4)_3$@C (LTP, prepared by a solvothermal method) and AC as the anode material and cathode material, respectively. Characterizations of LTP are given in Figure S10. CVs and charge-discharge curves of the LTP in Figure S11 demonstrate the compatibility with the 0.5 M Li_2SO_4-0.3 electrolyte. The LTP||0.5 M-Li_2SO_4-0.3||AC battery displays 65 mAh g^{-1} at a rate of 0.5 C (1C=130 mA g^{-1}) at -50 ℃ (Figure S12 a), corresponding to a 62 % capacity retention of 25 ℃. The LTP||0.5 M-Li_2SO_4||AC battery cannot work well at -50 ℃ (Figure S13). Similarly, we also assembled APIBs based on 1 M KCl and 1 M KCl-0.3 (adding DMSO with a mole fraction of 0.3 to the aqueous solution of 1 M KCl) as the electrolyte, organic polyimide (PI) and AC as the anode material and cathode material, respectively. CV and charge-discharge curve of the PI in Figure S14 present the excellent compatibility with the 1 M KCl-0.3 electrolyte. The PI||1 M-KCl-0.3||AC battery displays 58 mAh g^{-1} at a of 0.5 C (1 C=183 mA g^{-1}) at -50 ℃ (Figure S12 b), corresponding to a 62% capacity retention of 25 ℃. However, the PI||1 M KCl ||AC battery cannot work well at -50 ℃ (Figure S15). The performances of all the above mentioned fabricated batteries demonstrate that the novel electrolyte additive can realize a rechargeable AABs function and work well at ultra-low temperature of -50 ℃. The battery performance examination at low-T and high temperature, mentioned in this paper is executed in the low-T chamber and blast drying oven, which are shown in Figure S16, 17. To verify the universality of the novel additive, we added DMSO with a molar fraction of 0.3 to some common aqueous electrolyte, which containing lithium, sodium, potassium, and zinc salts independently, and placed the electrolyte at -50 ℃ for 2 hours. As a result, electrolytes with the novel additive did not freeze. Meanwhile, electrolytes without additive were all froze (Figure S18). It can be proved that the additive is universal. In short, the DMSO additive provides the possibility for the development of other aqueous battery at ultra-low temperature.

Last but not least, the interfacial/interphasial properties of electrode/electrolyte largely affect the battery performance. In the organic electrolyte system, the solid-electrolyte interphase (SEI) has an effect on the low-T performance of the battery.[22] For our aqueous electrolyte system, we tried to observe the presence of SEI on the electrode surface. According to the research on the interface layer (electrode/electrolyte) of aqueous battery by Wang's group,[23] we use electrochemical impedance spectroscopy(EIS), SEM, TEM, X-ray photoelectron spectroscopy (XPS) to study whether there are interfacial/interphasial layers in our battery system (the NTP||2M-0.3||AC system is selected for the study of the interface layer of electrode/electrolyte). Figure S19a, b and c are the impedance diagram of the full cell at 45 ℃, 25 ℃ and -50 ℃, respectively. For the batteries at 1st, 2nd, 5th and100th cycle, no additional semicircle is observed in the low frequency region. It indicates that no newly interface layer at electrode surface is formed during cycles. For the batteries at 100th cycle, the NTP anode surface information is analyzed by SEM, TEM and XPS. It was found by SEM that there is no significant change in the surface of the NTP anode after 100 cycles(Figure S20a). XPS is conducted on the NTP anode that recovered at the 100th cycle. The binding energies for the 1s valence electrons of O and C are shown in Figure S20c. Compared with the pristine electrode sheet, the new O1s signal can be attributed to the electrolyte salt $NaClO_4$. No change of C1s signal confirms that our battery system did not produce an electrode/electrolyte interface layer. It further suggests that the layer observed in the TEM image is carbon layer and not an interface layer(Figure S20b). In summary, a new interface layer is not formed on the electrode surface during the cycles.Therefore, the improvement of the low-T performance of AABs is only attributed to the addition of DMSO.

Conclusion

In conclusion, an electrolyte with ultra-low freezing point is designed by using DMSO as an additive with molar fraction of 0.3 for aqueous rechargeable batteries. The reason why the electrolyte shows that an ultra-low freezing point is demonstrated by spectral characterization and MD simulation. In the water/DMSO mixed electrolyte, HB network is formed via the combination of an oxygen atom in the S=O band and a hydrogen atom in the O-H band. Consequently, the inter-molecular HB between DMSO and water prevents the formation of tetrahedral structures of ice when the temperature drops to zero. The system with χ_{DMSO} =0.3 have most of the DMSO-Water HB in the form of 1DMSO-2Water, which explains why the lowest freezing point is realized when the DMSO molar fraction is 0.3. Benefiting from the additive, 2M-0.3 electrolyte exhibits a freezing point lower than -130 ℃, high ionic conductivity (0.11 mS cm^{-1}) at ultra-low T of -50 ℃. Based on such an electrolyte solvent, rechargeable NTP||2M-0.3||AC batteries, LTP||0.5M-Li_2SO_4-0.3||AC batteries, and PI||1M-KCl-0.3||AC batteries can work well at -50 ℃ and retain ~60% capacity of that at 25 ℃. Our study not only provides a new method for the development of low-T aqueous electrolyte, but also illustrates a new practical electrolyte system for aqueous batteries in future application.

Acknowledgements

This study was supported by the National Key R&D Program of China (2016YFB0901500, 2017YFA0206702); the National Natural Science Foundation of China (51771094, 21835004 and 21773226), Ministry of Education of China (B12015 and IRT13R30), and Tianjin High–Tech (No. 18JCZDJC31500).

Conflict of interest

The authors declare no conflict of interest.

Keywords: Aqueous batteries • low temperature • -50 ℃ • dimethyl sulfoxide • hydrogen bonds

[1] a) W. Ren, X. Chen, C. Zhao, *Adv. Energy Mater.* **2018**, *8(24):* 1801413; b) H. Gao, J. B. Goodenough, *Angew. Chem. Int. Ed.,* **2016**, *55(41):* 12768-12772*;* c) D. Bin, F. Wang, A. G. Tamirat, L. Suo, Y. Wang, C. Wang, Y. Xia, *Adv. Energy Mater.*, **2018**, *8(17):* 1703008; d)Y. Wang, J. Liu, B. Lee, R. Qiao, Z. Yang, X. Xu, L. Gu, Y. S. Hu, W. Yang, K. Kang, H. Li, X. Q.

Yang, L. Chen, X. Huang, *Nat.Commun.*, **2015**, *6:* 6401; e) C. Wessells, S. Peddada, R. Huggins, Y. Cui, *Nano Lett.*, **2011**, *11(12):* 5421-5425; f) J. Y. Luo, W. J. Cui, P. He, Y. Y. Xia, *Nat. chem.* **2010**, *2(9):* 760.

[2] a) Q. Nian, S. Liu, J. Liu, Q. Zhang, J. Shi, C. Liu, R. Wang, Z. Tao, J. Chen, *ACS Appl. Energy Mater.* **2019**, *2,* 4370−4378; b) H. Wang, H. Zhang, Y. Cheng, K. Feng, X. Li, H. Zhang, *Electrochim. Acta* **2018**, *278:* 279-289; d) L. Jiang, Y. Lu, C. Zhao, L. Liu, J. Zhang, Q. Zhang, X. Shen, J. Zhao, X. Yu, H. Li, X. Huang, L. Chen, Y. S. Hu, *Nat. Energy* **2019**, *4,* 495–503.

[3] a) S. S. Zhang, K. Xu, T. R. Jow, *J. Power Sources* **2003**, *115(1):* 137-140; b) S. S. Zhang, K. Xu, T. R. Jow, *Electrochem. Commun.*, **2002**, *4(11):* 928-932;c) Y. You, H. R. Yao, S. Xin, Y. X. Yin, T. T. Zuo, C. P. Yang, Y. G. Guo, Y. Cui, L. J. Wan, J. B. Goodenough, *Adv. Mater.*, **2016**, *28(33):* 7243-7248.

[4] a) C. Y. Wang, G. Zhang, S. Ge, T. Xu, Y. Ji, X. Yang, Y. Leng, *Nature* **2016**, *529(7587):* 515; b) Y. Ji, C. Wang, *Electrochim. Acta* **2013**, *107:* 664-674; c) G. Zhang, S. Ge, T. Xu, X. G. Yang, H. Tian, C. Y. Wang, *Electrochim. Acta* **2016**, *218:* 149-155.

[5] a) Y. Ren, C. Yang, B. Wu, C. Zhang, S. Chen, F. Wu, *Adv. Mater. Research,* **2011**, *287:* 1283-1289; b) M. Smart, B. Ratnakumar, K. Chin, L. Whitcanack, *J. Electrochem. Soc.* **2010,** *157(12):* A1361-A1374; c) X. Dong, Z. Guo, Z. Guo, Y. Wang, Y. Xia, *Joule* **2018**, *2(5):* 902-913

[6] a) S. Liu, G. R. Li, X. P. Gao, *ACS Appl. Mater. Interfaces* **2016**, *8(12):* 7783-7789; b) J. Zheng, M. Engelhard, D. Mei, S. Jiao, B. Polzin, J. G. Zhang, W. Xu, *Nat. Energy* **2017**, *2(3):* 17012; c) R. Wang, X. Li, Z. Wang, H. Zhang, *Nano Energy* **2017**, *34:* 131-140.

[7] a) L. Liao, T. Fang, X. Zhou, Y. Gao, X. Cheng, L. Zhang, G. Yin, *Solid State Ionics* **2014**, *254:* 27-31*;* b) K. Abraham, D. Pasquariello, F. Martin, *J. Electrochem. Soc*, **1986**, *133(4):* 661-666.

[8] a) D. Xu, Z. L. Wang, J. J. Xu, L. L. Zhang, X. B. Zhang, *Chem. Commun.* **2012**, *48(55):* 6948-6950; b) B. Sun, X. Huang, S. Chen, J. Zhang, G. Wang, *Rsc Adv*. **2014**, *4(22):* 11115-11120.

[9] D. B. Wong, K. P. Sokolowsky, M. I. El-Barghouthi, E. E. Fenn,C.H.Giammanco, A. L. Sturlaugson, M. D. Fayer, *J. Phys. Chem. B*, **2012**, *116(18)*: 5479-5490.

[10] J. E. Lovelock, M. W. H. Bishop, *Nature* **1959**, *183,* 1394-1395.

[11] R. N. Havemeyer, *J. Pharm. Sci*. **1966**, *55*, 851-853.

[12] D. H. Rasmussen, A. P. MacKenzie, *Nature* **1968**, *220,* 1315-1317.

[13] S. Ouyang, Z. Li, N. Wu, Z. Li, C. Sun, L. Fan *Spectrosc. Spectral Analysis* **2013**, *33*: 2425-2428.

[14] A. Bertoluzza, S. Bonora, M. A. Battaglia, P. Monti, *J. Raman Spectrosc.* **1979**, *8:* 231-235.

[15] F.Cansell, D. Fabre, J. P. Petitet, *Physica B: Condensed Matter* **1992**, *182*: 195-200.

[16] V. M. Wallace, N. R. Dhumal, F. M. Zehentbauer, H. J. Kim, J. Kiefer, *J. Phys. Chem. B* **2015**, *119(46):* 14780-14789.

[17] Y. C. Wen, H. C. Kuo, J. L. Guo, H. W. Jia, *J. Phys. Chem. B* **2016**, *120(51)*: 13125-13135.

[18] a) Q. Li, X. An, B. Gong, J. Cheng, *Spectrochim. Acta. A Mol. Biomol. Spectrosc* **2008**, *69(1)*: 211-215; b) S. Ouyang, N. Wu, J. Liu, C. Sun, Z. Li, S. Gao, *Chinese Phys. B* **2010**, *19*: 123101.

[19] B. Kirchner, M. Reiher, *J. Am. Chem. Soc.* **2002**, *124*, 6206-6215.

[20] U. Kaatze, R. Pottel, M. Schaefer, *J. Phys. Chem.* **1989**, *93*, 5623-5627.

[21] I. A. Borin, M. S. Skaf, *J. Chem. Phys.* **1999**, *110*, 6412-6420.

[22] a) L. Liao, X. Cheng, Y. Ma, P. Zuo, W. Fang, G. Yin, Y. Gao, *Electrochim. Acta* **2013**, *87*: 466-472; b) L. Liao, T. Fang, X. Zhou, Y. Gao, X. Cheng, L. Zhang, G. Yin, *Solid State Ionics* **2014**, *254*: 27-31.

[23] a) L. Suo, D. Oh, Y. Lin, Z. Zhuo, O. Borodin, T. Gao, F. Wang, A. Kushima, Z. Wang, H-C. Kim, Y. Qi, W. Yang, F. Pan, J. Li, K. Xu, C. Wang, *J. Am. Chem. Soc.* **2017**, *139(51)*: 18670-18680; b) C. Yang, X. Ji, X. Fan, T. Gao, L. Suo, F. Wang, W. Sun, J. Chen, L. Chen, F. Han, L. Miao, K. Xu, K. Gerasopoulos, C. Wang, *Adv. Mater*. **2017**, *29(44)*: 1701972.

10.1002/anie.201908913

WILEY-VCH

Entry for the Table of Contents

RESEARCH ARTICLE

An aqueous electrolyte with ultra-low freezing point is designed by using dimethyl sulfoxide (DMSO) as an additive, which makes aqueous alkali-ion (Li^+, Na^+, and K^+) rechargeable batteries (AABs) can work well at -50 ℃ and retain ~60% capacity when compared with that at 25 ℃.

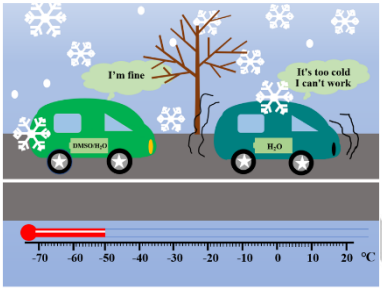

Q. Nian, J. Wang, S. Liu, T. Sun, S. Zheng, Y. Zhang, Z. Tao, and J. Chen*

Page No. – Page No.

Aqueous batteries operated at -50 ℃